

Orbital Decay of Supermassive Black Hole Binaries in Clumpy Multiphase Merger Remnants

Rok Roškar^{1*}, Lucio Mayer¹, Davide Fiacconi¹, Stelios Kazantzidis²,
Thomas R. Quinn³ & James Wadsley⁴

¹*Institute for Computational Science, University of Zürich, Winterthurerstrasse 190, CH-8057 Zürich, Switzerland*

²*Section of Astrophysics, Astronomy and Mechanics, Department of Physics, University of Athens, 15784, Zografos, Athens, Greece*

³*Astronomy Department, University of Washington, Box 351580, Seattle, WA 98195, USA*

⁴*Department of Physics and Astronomy, McMaster University, Hamilton, ON, L8S 4M1, Canada*

22 August 2018

ABSTRACT

We simulate an equal-mass merger of two Milky Way-size galaxy discs with moderate gas fractions at parsec-scale resolution including a new model for radiative cooling and heating in a multi-phase medium, as well as star formation and feedback from supernovae. The two discs initially have a $2.6 \times 10^6 M_{\odot}$ supermassive black hole (SMBH) embedded in their centers. As the merger completes and the two galactic cores merge, the SMBHs form a pair with a separation of a few hundred pc that gradually decays. Due to the stochastic nature of the system immediately following the merger, the orbital plane of the binary is significantly perturbed. Furthermore, owing to the strong starburst the gas from the central region is completely evacuated, requiring ~ 10 Myr for a nuclear disc to rebuild. Most importantly, the clumpy nature of the interstellar medium has a major impact on the dynamical evolution of the SMBH pair, which undergo gravitational encounters with massive gas clouds and stochastic torquing by both clouds and spiral modes in the disk. These effects combine to greatly delay the decay of the two SMBHs to separations of a few parsecs by nearly two orders of magnitude, $\sim 10^8$ yr, compared to previous work. In mergers of more gas-rich, clumpier galaxies at high redshift stochastic torques will be even more pronounced and potentially lead to stronger modulation of the orbital decay. This suggests that SMBH pairs at separations of several tens of parsecs should be relatively common at any redshift.

Key words: galaxies: evolution — galaxies: smbh — galaxies: mergers — galaxies: spiral — stellar dynamics

1 INTRODUCTION

The relationship between the masses of supermassive black holes (SMBHs) found at the centers of galaxies and the properties of their hosts is one of the fundamental relations in extragalactic astrophysics (e.g. Magorrian et al. 1998; Kormendy et al. 1997; Marconi & Hunt 2003; Häring & Rix 2004; Ferrarese & Merritt 2000; Tremaine et al. 2002; Gültekin et al. 2009; McConnell & Ma 2013; and references therein). The fact that a scaling between the two exists across multiple orders of magnitude suggests that their growth is governed by a common process (e.g. Peng et al. 2006; Merloni et al. 2010). Indeed SMBHs have been shown to be ubiquitous in hosts down to disc-galaxy mass scales locally (Greene et al. 2010), as well as at high redshift (Schawinski et al. 2012). There is also growing evidence supporting the presence of SMBHs in dwarf galaxies with stellar masses $\lesssim 10^9 M_{\odot}$ (Reines et al. 2011, 2013;

Koss et al. 2014). Combined with the Λ CDM hierarchical merging paradigm of structure formation, this implies that SMBHs should be present in a wide range of merging galaxy pairs. Consequently, one of the channels of SMBH growth is likely to be the coalescence of SMBH binaries.

The coalescence of the SMBH pair begins with the merging of the two galactic cores, followed by a stage where the two SMBHs form a coupled pair whose orbit decays due to the dynamical friction against the stellar and gaseous background, and finally down to parsec scales due to three-body scattering off individual stars (Begelman et al. 1980). Beyond the parsec scale, the decay proceeds due to gravitational wave emission (Baker et al. 2006). The lack of observed significant fractions of binary SMBHs or quasars implies that the entire process from the completion of the merger to coalescence must proceed rapidly. However, in the absence of gas, only 3-body scattering were responsible for the decay of the binary and reaching the gravitational-wave regime was not guaranteed due to the depletion of scatterers from the centre as the binary

* roskar@physik.uzh.ch

hardens (Milosavljević & Merritt 2001). Furthermore, even if the binary could decay efficiently, the timescale would be $\gtrsim 10^9$ yrs (e.g. Khan et al. 2012, 2013).

Such a decay scenario ignores the inevitable presence of large amounts of gas in the centers of merger remnants, which should give rise to SMBH pairs. High-luminosity systems observed locally show an abundance of gas near the nucleus often distributed in a disc-like structure (Sanders & Mirabel 1996; Davies et al. 2004a), often with associated star formation (Davies et al. 2004b). It is therefore clear that to model the decay of SMBH pairs, gas dynamics must be considered in addition to stellar dynamical processes.

In idealized models in which an SMBH pair was embedded in a gaseous and stellar background, Escala et al. (2004) found that the gaseous component provides the dominant torque for the decay of the binary, especially when the gas distribution is in a disc (Escala et al. 2005). Rapid orbital decay in the presence of a nuclear gas disc has also been confirmed in more realistic models of major mergers, where torques during the merger efficiently funnel gas into the central region, giving rise to a massive, dense nuclear disc ~ 75 pc in size (Mayer et al. 2007, 2008; Chapon et al. 2013). In these models, the decay timescale is extended for stiffer gas equations of state, but is typically found to be < 10 Myr. The rapid decay is primarily due to the strong dynamical friction against the dense nuclear disc. These results are not expected to be particularly sensitive to merger orientation (Escala et al. 2005) as long as the two SMBHs do not depart significantly from the gas disc reforming in the centre.

While much of the literature has focused on the rapid coalescence problem, some recent evidence points to the existence of binary SMBHs in systems undergoing the final stages of the merger, where the central region is heavily obscured (Fabbiano et al. 2011). The implication of these observations is that binary SMBHs may be common in luminous merger remnants, but were not previously observed due to obscuration. In this case, the process of orbital decay from 100 pc scale to 1 pc scale may actually take longer than previously considered.

If the ISM in which the SMBH pair is embedded is highly inhomogeneous, as is expected in the nuclear regions of galaxies (Wada & Norman 2001; Wada 2001), the torques exerted on the SMBH may be reduced. Nevertheless, Escala et al. (2005) found that the range of decay timescales increased by only factor of 3 for a reasonable span of ISM clumping factors. Recently, Fiacconi et al. (2013) modeled the orbital decay process in hydrodynamic simulations of SMBH pairs orbiting in a nuclear disc. Their nuclear discs were initialized to include clumps, whose mass spectrum is consistent with the mass spectrum of dense gaseous clouds typically found in galaxy centers. With the inclusion of disc inhomogeneities the SMBH binary orbit decay in these models becomes highly stochastic, depending on the gravitational interactions of the individual SMBHs with the clumps, which in many cases approach or even exceed the SMBH mass. The interactions between clumps and the SMBHs may accelerate or delay the decay, depending on the conditions of the interaction. In some cases, the resulting decay timescales were extended by as much as an order of magnitude. Their results highlight the fact that an inhomogeneous, multi-phase medium may play an important role in the sequence of events that eventually lead to the SMBH coalescence.

In this paper, we push this exploration further by attempting to model an inhomogeneous, multiphase ISM in a hydrodynamic simulation of an equal-mass merger. The initial conditions of our model are very similar to those of used in Mayer et al. (2007), but unlike in this previous work we move away from an idealized mod-

eling of the ISM based on an effective equation of state, and instead allow the gas to cool, form stars, and be affected by stellar feedback. These processes profoundly affect the nature of the central region immediately after the merger, qualitatively changing the orbital decay process.

This paper is organized as follows: in Sect. 2 we first briefly summarize the salient points regarding the simulation code GASOLINE, and then discuss in detail our modifications of the code; in Sect. 2.3 we describe the particle resampling method we use to increase the effective resolution of the simulation; in Sect. 3.1 we describe the morphological evolution of the merger remnant; in Sect. 3.3 we discuss the effect of the multiphase medium on the SMBH binary orbit evolution; we conclude in Sect. 4.

2 METHODS

2.1 Simulation Code

Our simulations are run using the Smooth Particle Hydrodynamics (SPH) code GASOLINE (Wadsley et al. 2004), which is an extension of the N -body treecode PKDGRAV (Stadel 2001). All analysis was performed using the open source PYNBODY package (Pontzen et al. 2013) and the IPYTHON environment (Pérez & Granger 2007). The simulation uses standard prescriptions for star formation from Stinson et al. (2006) using a Salpeter IMF. Star particles are spawned from a gas particle whose density $\rho > \rho_{\text{thresh}}$ and $T < T_{\text{thresh}}$, where ρ_{thresh} and T_{thresh} are density and temperature thresholds chosen such that the stars are forming in the densest, coldest gas regions found in the simulation. Due to the large dynamic range spanned by the simulation from the initial galaxy-scale stages to the final stages where we focus only on the inner regions, we have had to adjust these star formation parameters at different times. Initially, when the two merging systems are still distinct, we use a star formation density threshold $\rho_{\text{thresh}} = 0.1 \text{ amu cm}^{-3}$ and a temperature threshold $T_{\text{thresh}} = 1.5 \times 10^4 \text{ K}$. However, as the simulation progresses and the gas phase includes low-temperature, high-density material, we revise this prescription to $\rho_{\text{thresh}} = 10^4 \text{ amu cm}^{-3}$ and $T_{\text{thresh}} = 200 \text{ K}$. We discuss the multi-phase simulation technique and particle splitting in Sect. 2.3 below. Due to short timescales in the galactic centre, we also adjust the star formation timestep to 10^4 yr (for typical galaxy-formation simulations it is 10^6 yr).

The supernova feedback is the “blastwave” feedback from Stinson et al. (2006), which attempts to model the expansion of supernova-driven bubbles by mimicking the ballistic phase of the shock triggered by the supernova explosion. To mimic this phase, cooling is turned off for the timescale of the snowplow phase of the shock, calculated based on the instantaneous SN energy input and the ambient density. Such a feedback prescription overcomes the difficulty in distributing SN energy radiatively in the ISM; due to the implicit optically thin gas modelling and the high densities involved, the cooling timescales are extremely short. The blastwave feedback allows us to efficiently couple the SN energy to the ISM. In addition, the feedback model pollutes the gas with metals produced in SN Ia, SN II, and AGB stars.

In the simulations presented in this paper, we make use of the standard atomic hydrogen cooling function, which has a temperature floor at $\sim 10^4 \text{ K}$. We ignore contributions to the cooling function from metals above 10^4 K , which could have an impact on returning the gas expelled via feedback back to the central region. However, even with metal-line cooling, we expect the cooling timescales for 10^6 K coronal gas to be much longer than the

SMBH coalescence timescale (of order a few million years based on Mayer et al. 2007 and Chapon et al. 2013). Therefore, while not including the metal-dependent cooling may certainly influence the long-term post-merger evolution, we don't expect for it to significantly alter the properties of the rather short nuclear disk rebuilding phase covered in this paper. We allow the gas to cool below 10^4 K including metal lines using the empirical fit from Mashchenko et al. (2008) based on calculations by Bromm et al. (2001) until the gas is optically-thin to stellar radiation, and then switch to a novel thermal balance prescription for high density optically thick gas, as described in the next section.

2.2 Thermodynamics of the high density gas phase

The gas equation of state plays a decisive role in the fate of supermassive black hole binaries (Mayer et al. 2007, 2008; Chapon et al. 2013). In particular, the behaviour of the cold, high density, optically thick gas phase was poorly modeled in previous simulations adopting a prescribed equation of state. Here, we improve on previous work by including star formation in the coldest, densest gas, as well as stellar feedback, during all stages of the simulation. In addition, we implement a table for equilibrium temperatures based on Spaans & Silk (2000) appropriate for $\rho_{\text{gas}} > 0.1 \text{ amu cm}^{-3}$. The table gives an equilibrium temperature given a gas density following a detailed calculation including the relevant radiative processes in the densest gas phase. The model has been calibrated using 2D radiative transfer calculations for irradiated clouds in starburst environments Spaans & Silk (2000). These include stellar UV heating on dust and IR dust emission, photoelectric heating effect on dust, cosmic ray heating trapping of molecular and atomic lines in presence of a photodissociation layer and local turbulent velocity dispersion. The model is essentially an upgraded version of that adopted in Klessen et al. 2007. It assumes a star formation rate of $100 M_{\odot} \text{ yr}^{-1}$ when computing the UV flux from stars and ionization equilibrium between species.

In practice, we implement this cooling table as a temperature correction on top of the usual temperature calculation. If the particle's density is in the range described by the table, then we modify its temperature T_p by a factor $\Delta T = (T_{\text{eq}} - T_p)/T_{\text{eq}}$, where T_{eq} is the equilibrium temperature interpolated from the cooling table. In this way, the particles are pushed toward the equilibrium solution rather than simply assigned a temperature. Fig. 1 shows the temperature evolution of a single particle at different densities, for solar (top panel) and super-solar metallicity (bottom panel). The dashed lines show the cooling trajectories using our temperature correction, while the solid lines show the standard low temperature cooling. One can see clearly that the temperature correction initially accelerates the cooling, but as the gas gets colder it introduces a higher temperature floor at a given density. Essentially, this allows us to capture the reduced efficiency of cooling in regions of high optical depth in the very inner, dense region of our system, without having to resort to a full radiative transfer calculation. Note that the temperature correction is applied after the energy calculation, so as to make sure that the cooling still takes place at a reasonable rate.

In Fig. 2 we show the phase diagram using this low temperature cooling correction. We chose an output at the moment of the final apocentre, when the softening is reduced to 1 pc to ensure that the high-density end of the distribution is well-populated. The blue and green lines show the modified cooling table values for Z_{\odot} and $3Z_{\odot}$ respectively.

Since we are concerned with modeling the inhomogeneous

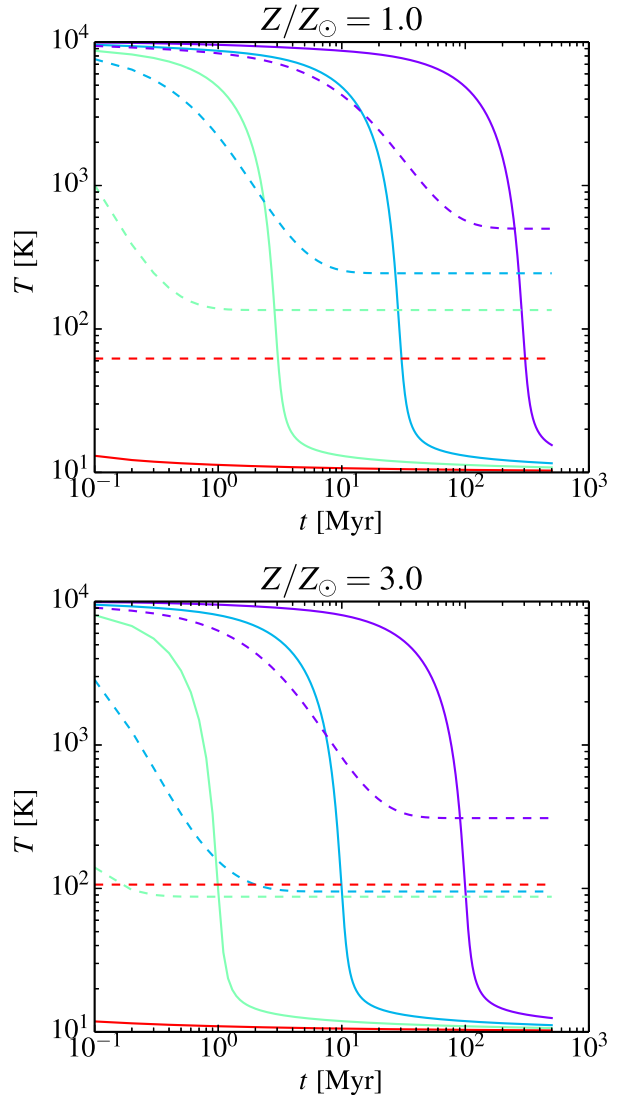


Figure 1. Temperature evolution of a single particle using the standard low-temperature cooling curve (solid lines) and our temperature correction using calculations from Spaans & Silk (2000) (dashed lines). Purple, turquoise, green and red colours represent densities of 1, 10, 100 and 10^4 amu cm^{-3} respectively.

ISM and we are allowing the gas to cool to low temperatures, we must take care to guarantee that any fragmentation remains physical. We ensure that the gas particle's implied Jeans scale is resolved at a given temperature and density by imposing a pressure floor constraint following Agertz et al. (2009). The minimum pressure is set to $P_{\text{min}} = \epsilon G h^2 \rho^2$, where $\epsilon = 3.0$ is a safety factor, G is the gravitational constant, h is the smoothing length and ρ is the particle density. In Fig. 3 we show the distribution of the ratios of $M_{\text{jeans}}/M_{\text{part}}$ during the final part of the simulation when the force resolution is 1 pc, showing that the Jeans mass is resolved by $\gtrsim 10$ particles everywhere in the simulation are resolved and therefore any fragmentation and clumping we see is physical.

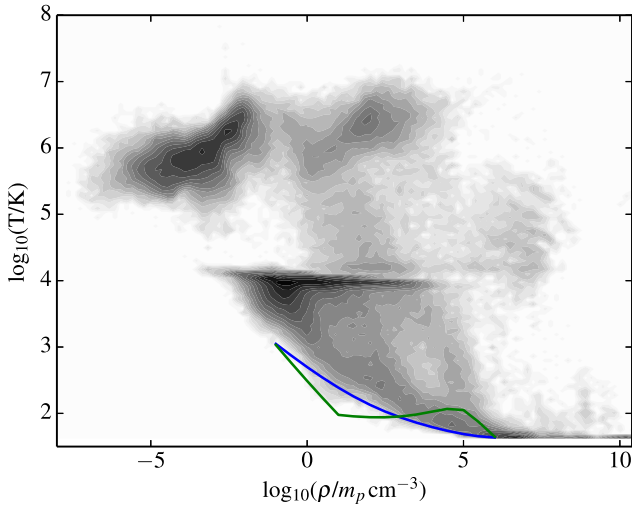


Figure 2. Phase diagram for the gas during the final stages of the simulation. The blue and green lines delineate the gas equilibrium from Spaans & Silk (2000) for low ($Z < Z_{\odot}$) and high ($Z > Z_{\odot}$) metallicities respectively.

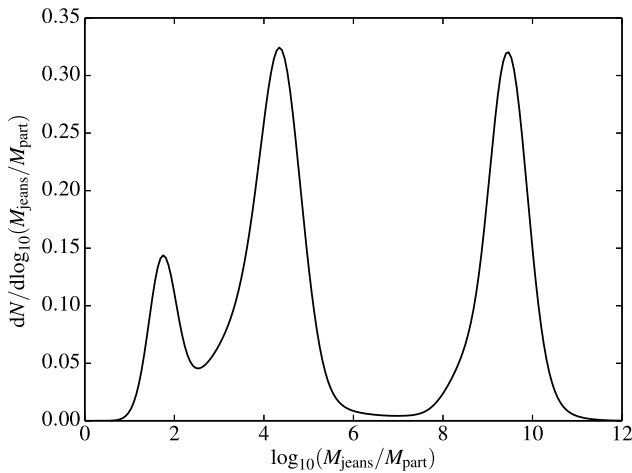


Figure 3. Ratio of particle mass to local jeans mass during the final stage of the simulation. Our imposed pressure floor ensures that the local jeans mass M_{jeans} is always resolved by approximately 10 particles, ensuring that any clumping we see in the simulation is physical.

2.3 Particle Resampling during the Galaxy Merger

The system is initialized as a merger between two Milky Way-like discs each with a SMBH particle embedded in the centre. The same initial conditions were used as a starting point for the simulations presented in Mayer et al. (2007). The initial systems are equilibrium discs sampled with 10^5 gas particles and 2×10^5 star particles (10^5 particles in the disc and the same number in the bulge) embedded in dark matter halos with 10^6 particles. The particle masses are $4 \times 10^4 M_{\odot}$ for gas and $8 \times 10^4 M_{\odot}$ for star and dark matter particles. The masses of the three components in each of the initial discs are $4 \times 10^9 M_{\odot}$, $4 \times 10^{10} M_{\odot}$, and $1 \times 10^{12} M_{\odot}$ for gas, stars, and dark matter respectively. With these choices the resulting galaxy model is a typical massive late-type spiral, consistent with the predictions of abundance matching at $z = 0$ (e.g. Behroozi et al. 2013) and having a moderate but typical gas fraction in the disc for Sb/Sc galaxies of 10%. Both galaxies host a SMBH

modeled as a collisionless particle of $2.6 \times 10^6 M_{\odot}$ embedded in a bulge of $8 \times 10^9 M_{\odot}$. The initial softening lengths are 100 pc for all particle species. Note that we use several species of dark matter particles in order to increase the effective resolution in the inner regions. We have verified that the individual discs are in acceptable equilibrium by evolving them in isolation for several Gyr. The centres of the two halos are initially separated by > 500 kpc and the two systems are on an in-plane parabolic orbit with a pericenter of 50 kpc, appropriate for a cosmologically-motivated merger geometry. Star formation and feedback are turned on from the beginning in order to provide a multi-phase gas medium and a variety of stellar populations, which are crucial for the modelling of the state of the central region just after the merger.

We stop the simulation just before the second passage (at approximately 4.9 Gyr), when the two cores are separated by ~ 5 kpc. We define a spherical region of 35 kpc around the merger remnant for particle resampling. This is sufficient to ensure that the boundaries will not interfere with the centre on timescales of interest (~ 100 Myr). We split these “parent” particles into eight “child” particles and distribute them randomly according to the SPH smoothing kernel around each parent. The child particles receive $1/8$ of the mass of their parents and inherit the same velocity, ensuring that we conserve mass and angular momentum in the system. We compute the densities of the child particles according to the kernel, but we distribute other simulation quantities (temperature, metals, feedback information etc.) to the child particles via the standard SPH scatter scheme. For this final step, we restrict ourselves to computing the gather radius using only 16 neighbors in order to prevent excessive blurring of boundaries in the flow. Using this technique we attempt to minimize the introduction of random noise that would result from a more crude resampling of the multiphase medium. The softenings at this stage are set to 50 pc for the stars and gas. The resampled system includes 7.3×10^5 gas, 3.8×10^6 star, and 2.5×10^5 dark matter particles. Note that like in Mayer et al. (2007), we do not split the dark matter particles, although we do split the star particles. The particle splitting is accomplished in part by reusing routines from SKID¹ (Stadel 2001) to compute the densities and neighbor lists for the gather-scatter scheme.

Fig. 4 shows the system on several different scales just after the splitting. The left panel shows the resampled region. The two nuclear disc cores are easily identifiable in the middle panel, which also clearly shows the turbulent nature of the gas. The rightmost panel zooms in on the central region, showing the dense disc around one of the SMBHs about 500 pc across.

During the initial stages of the merger, the SMBHs stay within a softening length of the potential minimum of the parent disc. However, when we move to higher resolution, this displacement could have an effect on the efficiency of the pairing, since we are also changing the force resolution. In order to prevent the SMBHs from leaving the centers of their respective host cores due to this change in resolution, we move the SMBHs to match the centre of mass and velocity of their respective discs. For this recentering, we determine the center of mass and velocity of particles within a 1 kpc sphere around each SMBH.

A final modification of the simulation is done at the last apocentre passage before the completion of the merger. At this point we increase the force resolution to 1 pc for the gas particles and the SMBH particles in order to allow for the possibility of the

¹ <https://hpcforge.org/projects/skid/>

SMBH orbits decaying to the parsec scale, in a similar fashion as in Mayer et al. (2007) and Escala et al. (2004). The stars which have already formed keep their softening, but newly formed stars have the softening of their parent gas particles. This results in a mismatch between the mass and force resolution in the stellar component. However, we expect the most important contribution to dynamical friction to come from particles closest to the SMBHs, i.e. those in the nuclear discs. This means that for the purposes of the orbital evolution, the newly formed stars and the gas particles will have the largest effect and those both have resolution of 1 pc. Just as in the particle splitting step, we recentre the SMBHs with respect to the centre of mass and bulk velocity of their surrounding gas. After this final refinement, the simulation is evolved until the SMBH orbit decays down to the scale of the softening length.

3 RESULTS

3.1 Post-Merger Phase

During the final passages before the completion of the merger, the two cores undergo substantial starbursts breaking up the homogeneity of the ISM. These starbursts, reaching star formation rates of $\sim 80 M_{\odot} \text{ yr}^{-1}$, have the effect of blowing out the gas from the central region, delaying the formation of the nuclear disc for the final SMBH orbit decay. Fig. 5 shows an edge-on map with the velocity field overlaid just before the final pericentre. The supernova-powered winds stir the gas surrounding the central disc, causing asymmetric outflows and inflows, as is clearly seen below the plane. We consider the merger to be complete when the two cores fully merge, which occurs at time $t = 5001$ Myr since the start of the simulation. In the following analysis, we denote times in terms of the time elapsed since the completion of the merger in units of the orbital time, τ , measured at 100 pc.

In Fig. 6, we show a single output at several different scales, just after the two cores have fully merged. On the scales of tidal tails (several kpc), we can see that the gas structure is not smooth but has instead become clumpy and disordered due to the multiphase nature of the ISM. In the inner region, the gas structure is highly irregular at this stage, without any clear evidence of ordered bulk motion. Furthermore, although the gas is funneled into the centre the star formation rate remains at several $M_{\odot} \text{ yr}^{-1}$ and within several 10^7 yrs much of the gas that makes it to the centre is depleted, as can be seen in the bottom two panels of Fig. 7, due to feedback and star formation.

The violent nature of the final encounters breaks the in-plane symmetry of the merger, manifested in the misalignment of one of the discs with respect to the xy plane as can be seen in the top right panel of Fig. 7. The left and right column pairs of the figure show face-on and edge-on projections respectively at different times. Although we took care to set the SMBH into the centre of mass and velocity of their respective cores at the final resampling, it is clear that they are easily tossed out of the plane. This most likely results from interactions with the massive clumps, which in many cases exceed the mass of the SMBHs. To quantify the importance of dense clumps, we use the group finder SKID (Stadel 2001) to obtain groups of gravitationally bound particles in every output. We set a mean density threshold to $\rho_{\min} = 2 m_p \text{ cm}^{-3}$ and a linking length for the Friends-of-Friends algorithm to five times the minimum softening length, i.e. $\tau_{FF} = 5$ pc. Note that we use both, gas and stars in clump identification and ρ_{\min} pertains to density calculated from both particle species. The density threshold ensures that

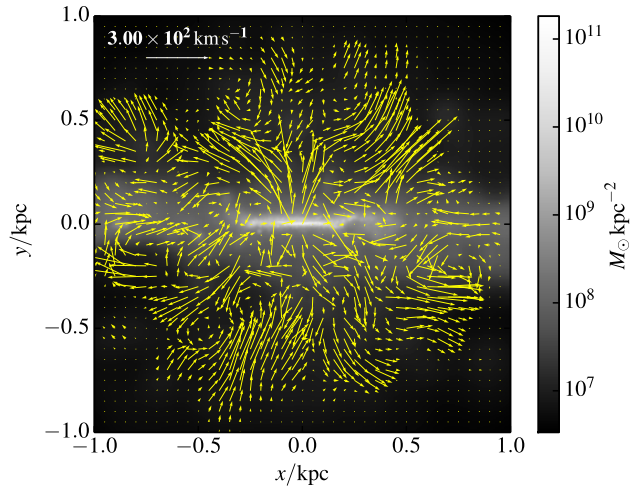


Figure 5. Density map shortly after the merger with velocity overlaid. The velocity field is generated for a thin slice, while the map is showing a projected column density. Supernova-powered outflows from the central region with velocities of several hundred km/s are not uncommon.

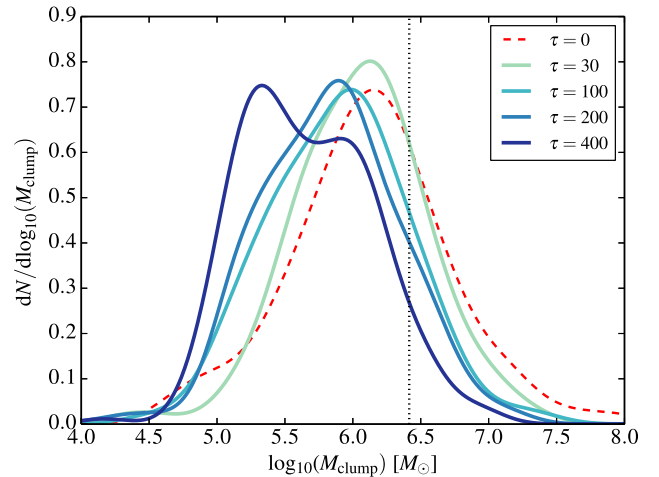


Figure 8. Clump mass distributions at four different times. The vertical line marks the mass of the SMBHs.

we only identify the dynamically most interesting, densest particle groups. We show the resulting clump mass distributions at several representative times during the system’s evolution in Fig. 8. The vertical dashed line indicates the mass of the SMBH particles, which some of the clumps clearly exceed, in particular immediately after the merger. At that time, many of the clumps are quite gas-rich, but due to the high densities they quickly convert much of their mass to stars. The clumps therefore quickly become akin to dense star clusters rather than gas clumps. We discuss the impact of these massive clumps on the SMBH orbital decay in Sect. 3.3.

3.2 Disc Rebuilding Phase

The central region quickly (in a few Myrs) recovers from the starburst and the circumnuclear disc begins to reform. Fig. 9 shows the time evolution of stellar and gas density profiles in the central 100 pc (top panel) and the radial dependence of $z_{\text{rms}} = \frac{1}{N} \sqrt{\sum_{i=0}^N z_i^2}$ (non-parametric proxy for thickness; bottom panel)

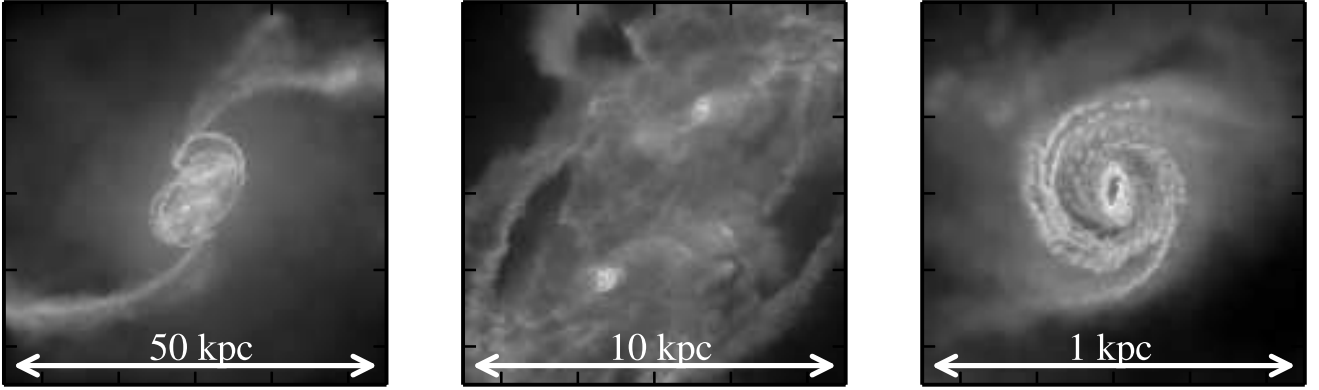


Figure 4. Maps of the gas density of the system just before the final stage of the simulation. The two cores are clearly visible and the SMBHs are embedded in their centers.

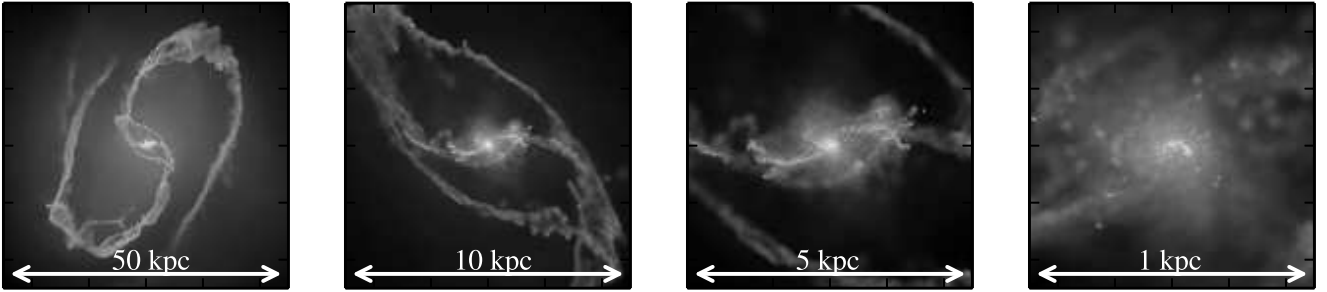


Figure 6. Sequence of face-on projections of the gas distribution at $t = 5003$ Myrs ($\tau \sim 10$, where τ is time elapsed in units of orbital time at 100 pc), just after the two cores become fully merged. The tidal tails are broken up due to feedback and multiphase ISM, reducing the efficiency of accretion into the central region.

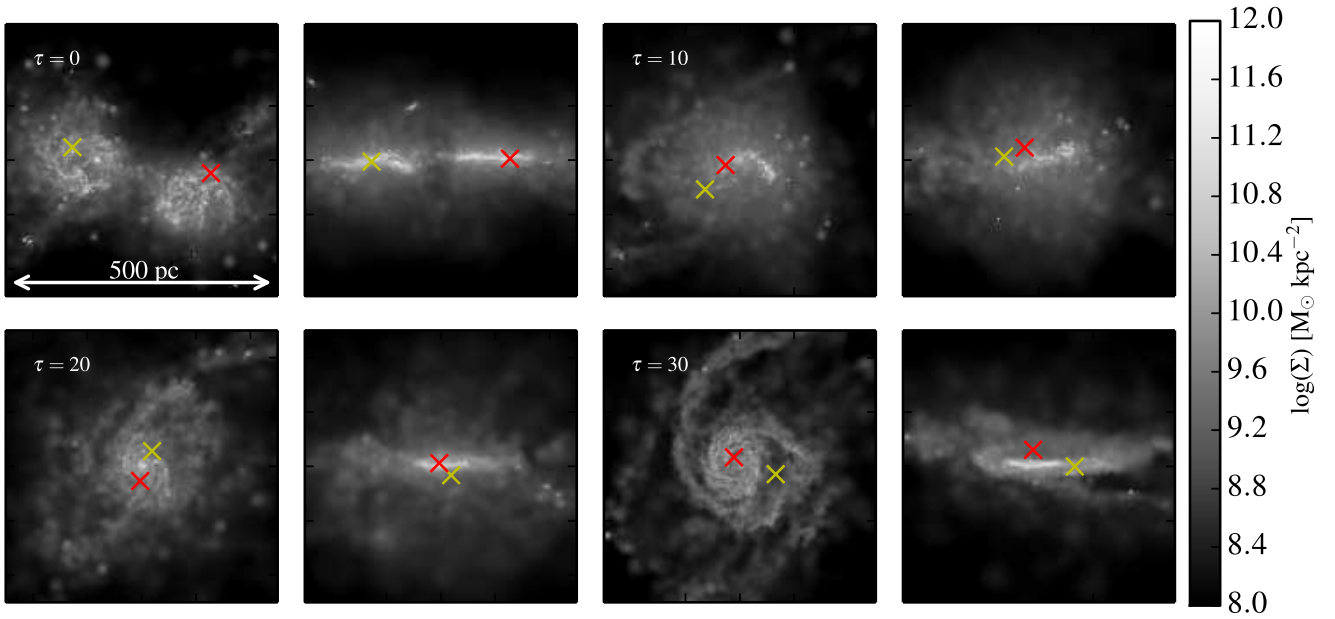


Figure 7. Face-on and edge-on gas density projections at several times during the final phase of the merger, after the last apocentric passage. The two SMBH particles are indicated by yellow crosses.

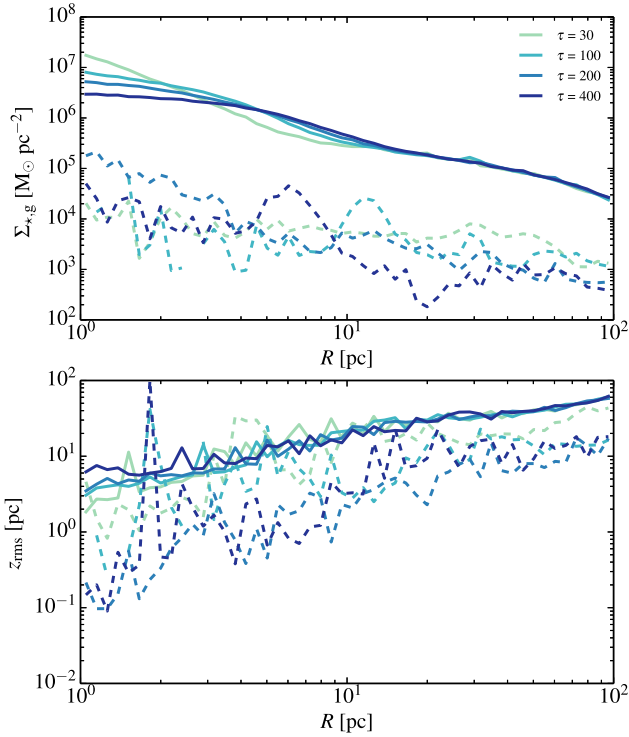


Figure 9. Density and z_{rms} as a function of radius (top and bottom panels respectively) for stars (solid) and gas (dashed) at four representative times, as indicated.

at different times. Owing to a period of intense star formation during the merger, the stellar density here exceeds the gas density by a factor of 100-1000. This is very different than the situation explored in previous studies where the nuclear gas disc dominated the mass distribution (e.g. Mayer et al. 2007). Furthermore, while a nuclear disc does form, the accretion is hindered by the fact that much of the mass is locked up in massive clumps. As can be seen from Fig. 8, the clumps form even at late times (although their masses decrease somewhat), continuously stirring the disc and affecting the orbital decay of the SMBH binary. In most cases, the dense gas clumps at early times convert most of their mass into stars but remain gravitationally bound and only slowly get disrupted. Note that due to the short timescales in question (< 10 Myr) to form the clumps and convert them into stars, the supernova feedback has little effect on regulating the clump masses.

Fig. 10 shows the ratio between rotational velocity v and velocity dispersion σ of the gas disc, quantitatively demonstrating the disc rebuilding phase. Immediately after the merger ($\tau = 0$ and $\tau = 10$), $v/\sigma < 2$, indicating lack of rotational support and ordered bulk motion throughout the central region. However, after just 4 Myr $v/\sigma > 2$ in the interior 300 pc and by 10 Myr after the merger is complete, the inner several hundred parsecs contain a rotationally-supported, kinematically cold gas disc. Nevertheless, the gaseous disc remains much less massive than the stellar component (Fig. 9).

The gaseous and stellar discs are significantly flared, as shown by the strong evolution of z_{rms} (model-independent proxy for scale height) as a function of radius at all times. While the thickness of the stellar component remains largely fixed throughout the 80 Myr of evolution, however, the decrease in the thickness of the gas component is evident especially in the inner regions. This is due to the

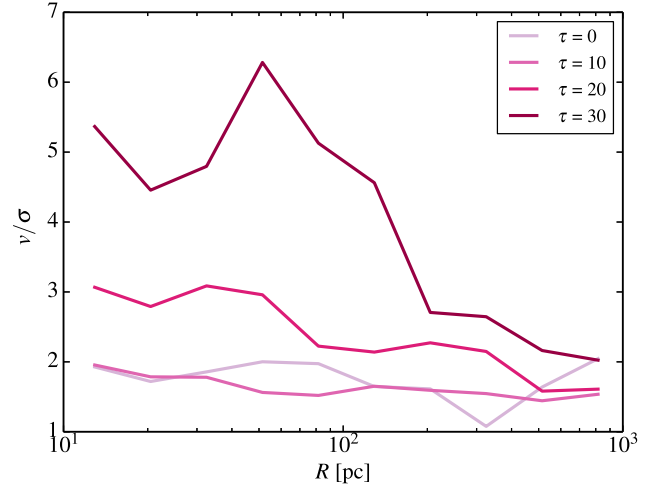


Figure 10. The ratio of tangential velocity v to velocity dispersion σ at several times shortly after the merger is complete. The disc rebuilds on a timescale of $\sim 10^7$ years, evidenced by the rapid rise in v/σ , and extends out to ~ 200 pc.

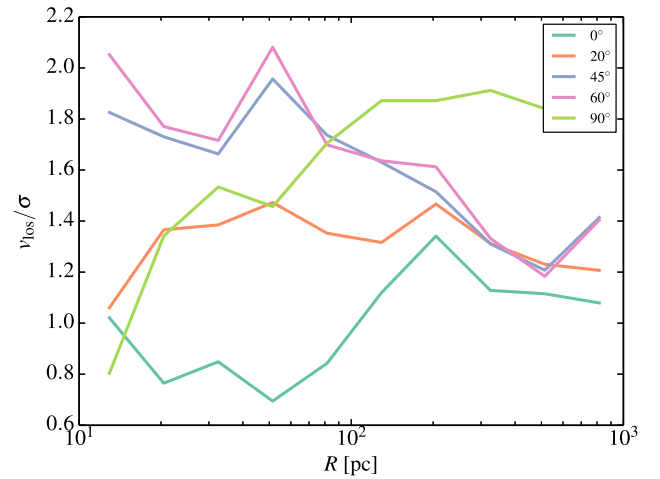


Figure 11. v_{los}/σ , where v_{los} is the mean velocity along the line of sight. Colours represent different inclinations of the central disc. The output shown is at $\tau = 30$ ($t = 5007$ Myr).

accumulation of gas in the central region as the disc reforms and the chaotic merger-induced disc structure settles down.

Fig. 10 shows the most “optimistic” measure of v/σ , which is calculated simply as the ratio of the average tangential velocity component and the velocity dispersion in each radial bin. However, observationally, v/σ is typically measured from the line-of-sight velocity and the associated velocity dispersion based on spectral line shift and width respectively. We crudely model this type of v/σ determination in Fig. 11, showing v_{los}/σ for a range of inclination angles (0 corresponds to face-on) at $t = 5011$ Myr. The majority of v_{los}/σ values lie in the range of 1-2, which signifies a thickened, highly turbulent disc.

In a recent study targeting 17 local (Ultra) Luminous Infrared Galaxies (ULIRGs), Medling et al. (2014) found that in most cases (16 out of 18 nuclei) they contain a dense nuclear disc composed of gas and stars. The observed discs mostly have effective radii of a few hundred parsecs and dynamical masses estimated in the

range of $10^8 - 10^9 M_\odot$. The stellar populations appear young (ages < 10 Myr), implying that they are associated with in-situ star formation in the nuclear discs themselves, analogous to the disc in our simulations. Furthermore, they find that v/σ in their sample ranges from 1-2, in good agreement with the values in Fig. 11. We can therefore be reasonably confident that we are capturing some of the essential processes of the nuclear disc rebuilding.

3.3 SMBH Orbital Decay

In the previous section we highlighted some of the most important aspects of the morphological evolution of the merger remnant. The morphology and the nature of the gas dynamics are critical for the evolution of the SMBH binary. A prominent feature of the merger in our simulation is that although in the initial conditions the system lies in a single plane, this symmetry is broken during the final stages of the merger (Fig. 7). As discussed above, this phase is accompanied by the formation of massive clumps which additionally perturb the SMBH orbits. The combination of these effects induces significant vertical motion in the orbits of the two SMBHs with respect to the the plane of the disc that is reforming after the merger and it means that they both feel a much smaller drag on their orbits around the centre compared to previous models (e.g. Mayer et al. 2007).

We have traced the evolution of massive clumps from one output to another to determine their potential impact on the SMBHs. The time between successive outputs is 50k years which means we can accurately trace the orbits even in the innermost regions. We find that while most clumps remain far enough that they do not have a significant impact on the SMBH orbits, there is a small but important number of clumps that come within 5-10 pc of the two SMBH particles. This results in a random forcing on the orbits of the SMBHs which serves to work against the drag from dynamical friction and helps keep one of the SMBHs orbiting well out of the plane of the main disc. The ratio of the SMBH velocity to the acceleration experienced due to an individual clump, i.e. $v_{\text{bh}}/a_{\text{clump}}$ gives a timescale for velocity change $\Delta v \propto v$. We find that this timescale is less than a Myr for a number of clumps, suggesting that the random forcing from clumps is significant for the orbital evolution of the SMBH pair.

We show the orbital evolution of the SMBH binary after the final apocentric passage in Fig. 12. As described above, the aftermath of the merger destroys the plane-symmetry of the system and excites the out-of-plane oscillations of the two SMBHs (at ~ 5002 Myr). Because the densest component (stars and gas) is distributed in a disc, the increased vertical oscillations result in drastically reduced dynamical friction and therefore the SMBH orbital decay timescale is extended. One of the SMBHs continues to decay its orbit, albeit slowly, while the other remains at essentially a fixed oscillation from the centre (Fig. 12, bottom panel).

The decay (especially in the vertical oscillation amplitude) of the binary continues until at ~ 5023 Myr one of the SMBHs (blue) begins to orbit within the misaligned nuclear disc. As it nears the centre, it encounters a weak stellar bar which measures a few parsec across. The SMBH particle orbit is strongly torqued by the small bar and it loses all of its angular momentum very rapidly, becoming pinned to the potential minimum at the centre. The other SMBH particle (orange) continues to experience random forcing from the clumps (possibly also by spiral waves), and is therefore unable to sink to the center until the clumps have largely dissolved several tens of Myr later. We have estimated the dynamical friction timescale due to only the background density (using calculations

similar to those in Fiacconi et al. 2013) in the inner bulge to be ~ 50 Myr, so the random forcings due to the clumpy medium increase this timescale by a factor of ~ 2 . Note that during this time the SMBHs are moving supersonically through the gaseous background at typical mach numbers of 2-3. In principle this should amplify the drag (Ostriker 1999; Chapon et al. 2013), but the density of the gaseous background is sufficiently low that the resulting dynamical friction does not dominate the evolution.

The dotted lines in the bottom panel of Fig. 12 show the vertical scale height of the stellar component at 5, 10 and 50 pc (bottom to top; see Fig. 9). During the period that the decay of the second SMBH (orange line) seems stalled, the vertical oscillations of the orbiting SMBH are beyond the vertical scale height of the disc. Since much of the mass is concentrated in the disc plane, these vertical excursions mean that the drag on the SMBH orbit is reduced. Furthermore, dynamical friction against the gas is more efficient where the bulk motion is highly ordered, which is not the case outside the disc. The final decay is shown on the inset axes in the top panel.

During the last few Myr of the decay, the orbit of the second SMBH is eccentric with $e = (r_a - r_p)/(r_a + r_p) = 0.7$ and just before the binary decays to our resolution limit $e \sim 0.4$. This is consistent with Fiacconi et al. (2013), where it was found that for in the SMBH decay with a clumpy ISM, the orbits remained eccentric down to the resolution limit. The fact that the binary approaches the gravitational wave regime before circularizing can be critical for the subsequent gravitational wave emission (Mayer 2013).

Finally, an important caveat in the evolution of the SMBH binary is the fact that our simulation does not include the effects of BH accretion and associated AGN feedback. We perform a crude estimate of the expected accretion rate assuming spherical accretion and taking into account the relative velocity between the black hole and the background

$$\dot{M} = \frac{4\pi G^2 M_\bullet^2 \rho}{(v_{\text{rel}}^2 + c_{\text{s,turb}}^2)^{3/2}}, \quad (1)$$

where M_\bullet is the mass of the SMBH, v_{rel} is the relative velocity between the SMBH and the background, $c_{\text{s,turb}} = (c_s^2 + \sigma^2/3)^{1/2}$ is the turbulent sound speed with σ the gas velocity dispersion and G is the gravitational constant. Insofar as the SMBH particles can be considered as test particles sampling the potential in the inner part of the galaxy, we approximate v_{rel} as the velocity dispersion of the stellar component which during the time shortly after the merger is ~ 200 km/s. The resulting Bondi rates are $\sim 0.05 - 0.1 M_\odot \text{ yr}^{-1}$. This means the BHs could double their mass during the ~ 100 Myr of decay phase in the nuclear disk, which would have only a marginal effect on dynamical friction as well as on the exchange of energy and angular momentum via stochastic torquing. Using these approximations and assuming that the luminosity of the nuclei is given by $L = \epsilon_r \dot{M} c^2$ where ϵ_r is $\sim 10\%$ from both observational constraints and models of viscous accretion disks. With these assumptions, we estimate that, for the typical gas densities encountered by the SMBHs (recall that the SMBHs oscillate significantly above and below the disk plane) the expected luminosities would be $< 0.1 L_{\text{edd}}$, i.e. $\sim 10^{43} \text{ erg s}^{-1}$. Of this accretion luminosity only a very small fraction would couple to the ISM, thermally and/or via momentum transfer. While the coupling mechanism and efficiency is largely unknown, simulations that attempt to reproduce the observed correlations between SMBH masses and host galaxy properties require a coupling efficiency $\epsilon_{fb} \sim 0.005 - 0.05$, where the wide range of values is explained by the dependence on the specific thermodynamical model of the ISM that simulations adopt

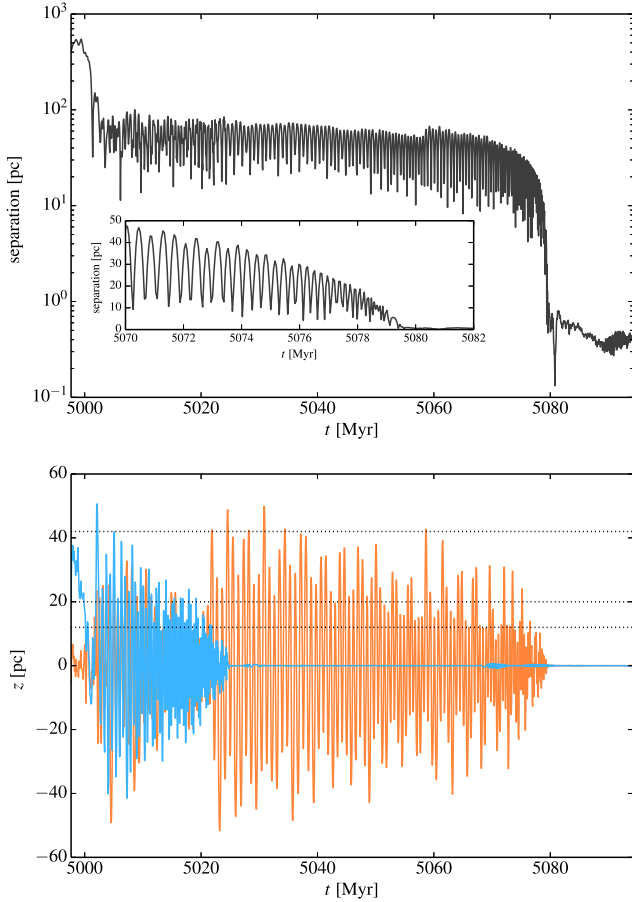


Figure 12. **Top:** Separation of the SMBHs as a function of time starting at approximately the last apocentre, i.e. the time when we switch to 1 pc spatial resolution. The inset shows the last stage of the decay. **Bottom:** Motion perpendicular to the plane for each SMBH (shown with different colours). From top to bottom, the dotted horizontal lines show the z_{rms} of stars at 50, 10, and 5 pc.

(see e.g. Springel et al. 2005; Callegari et al. 2009). Therefore, we can assume the luminosity actually coupled with the gas will be $< 10^{42}$ erg/s. We can compare this upper limit with the energy actually released into the ISM by supernovae type II via our blastwave feedback recipe during the phase of SMBH decay in the nuclear disk. This amounts to $\sim 10^{42}$ erg/s. This is a conservative estimate since it does not include the energy released by SN type I, which we include as thermal energy injection into the ISM in the simulations but allow it to be radiated away rather than modeling it with a blastwave (see Stinson et al. 2006). Overall, these calculations suggest that the impact of AGN feedback in the SMBH decay phase studied in this paper would be modest since it will likely deposit less energy than supernovae feedback. Of course there are huge uncertainties in how to model the various feedback processes in the first place. However the main point here is that we are already depositing a significant amount of thermal energy into the ISM with our feedback model, hence the existence of a prominent cold clumpy phase in the nuclear disk should be viewed as a fairly robust outcome.

4 CONCLUSIONS

We perform a multi-scale simulation of an equal-mass merger of two spiral galaxies with an SMBH embedded in each of the progenitor’s centers. As the merger nears completion, we increase the resolution of the central region via a particle splitting method, taking care to ensure that the thermodynamic state of the gas and the instantaneous properties of the feedback processes are preserved. Throughout the simulation, our model includes star formation and stellar feedback, establishing a multiphase, turbulent ISM in the central region. After the two cores successfully merge and the effects of the nuclear starburst subside, a nuclear disc grows in the centre of the merger remnant in the span of a few Myr, eventually reaching a size of ~ 400 pc. The two SMBHs form a loose binary at this point, but the violent nature of the late stages of the merger causes their orbits to have a considerable motion perpendicular to the disc plane. This delays the eventual complete decay of the SMBH binary which takes approximately 80 Myr. This decay timescale is comparable to that found in recent idealized experiments (supplemented by analytical estimates) by Fiacconi et al. (2013) and almost two orders of magnitude longer than found in previous studies of analogous systems that used an effective equation of state to model the gas (Mayer et al. 2007).

Our results indicate that SMBH pairs may decay to parsec scales on a much longer timescale than previously thought. If we consider the timescale ~ 100 Myr to form a tight binary from a separation ~ 100 pc as typical, galaxies that show morphological signatures of a recent merger (e.g. tidal tails) with a post-starburst stellar population might be the most appealing candidates to look for SMBH pairs. However, this timescale is subordinate to the dynamics of the SMBH pair in the inhomogeneous background and to the eventual presence of massive enough clumps formed during the merger. Moreover, it is worth recalling that the stochastic character of the dynamics outlined by our results may also accelerate the orbital decay process. Fiacconi et al. (2013) estimated a threshold mass \mathcal{M}_* below which a SMBH orbiting in such an environment might be dynamically influenced by massive clumps. Although it was only an order of magnitude estimate, a typical value $\mathcal{M}_* \sim 10^7 M_\odot$ is fairly consistent with our results and with a recent discovery of SMBH pair by Fabbiano et al. (2011). This mass roughly corresponds to a bulge mass $\lesssim 5 \times 10^9 M_\odot$, according to the scaling relation between SMBH and bulge masses (Sani et al. 2011). This suggests an additional conservative selection criterion: SMBH pairs might be more easily detected in late-type (hence relatively gas-rich even at $z = 0$) galaxies with stellar mass $\lesssim 10^{10} M_\odot$, although the occupation fraction of SMBHs at such low masses is still unclear.

Nevertheless, these considerations still neglect the details of the dual AGN activity required for the SMBHs to be detected (Van Wassenhove et al. 2012, 2014). Just after the merger phase, obscuration might be relevant or the central gas might be depleted after the starburst and mostly accumulated in to massive clumps, reducing the time during which the SMBHs could be active at the same time. Our simulations here do not include a model for SMBH accretion and AGN feedback, which would be critical for determining reasonable observability constraints.

The simulations presented here used galaxy models that were tailored to reproduce low-redshift late-type galaxies. This was motivated primarily by the need to compare with previous work using similar initial conditions (e.g. Mayer et al. 2007). Furthermore such systems host moderate mass SMBHs, which would be the preferential target of future gravitational wave experiments such as eLISA

making our choices of broader relevance. However, since galaxy mergers are much more frequent at higher redshift, future work will have to explore mergers between galaxies whose properties are more akin to high- z galaxies. The latter will be needed to assess the likelihood of finding SMBH binaries at tens of parsecs to a few parsecs separations as well as being more relevant to make predictions for rates of gravitational wave emission events originating from coalescing massive BH binaries. Qualitatively, we can expect that the stochastic orbital decay regime found here will be even more relevant because at $z > 1$ galaxies with stellar masses comparable to the Milky Way appear to be more gas-rich as well as clumpier even when they are not in a merging phase (Genzel et al. 2006; Elmegreen et al. 2009). Clumps observed in high- z galaxies are also much more massive, up to a few $10^8 M_{\odot}$, which would imply stronger gravitational forcing of the massive BHs during encounters, potentially leading to even larger delays in the orbital decay. As shown by Fiacconi et al. (2013), the larger mass scale of the clumps also means stochastic torques will affect comparatively more massive BHs, in the range $10^7 - 10^8 M_{\odot}$. Such gas-rich, clumpy massive disc galaxies at $z > 2$ with relatively massive central SMBHs are likely the progenitors of massive elliptical/S0 galaxies today, hence the stochastic torquing regime may be particularly relevant to understand the dynamical evolution and mass growth of the most massive SMBH found in the current Universe.

While quantitative statements cannot be made at this stage, it is rather plausible that dual AGNs with separations of tens of parsecs should be quite common at $z > 1$ due to combination of long orbital decay timescales implied by a clumpy ISM, perhaps exceeding 100 Myr, and the large gas reservoirs as well as highly dynamical environments leading to efficient gas inflows and accretion onto SMBHs (e.g. Bournaud et al. 2012). The dense gaseous environments expected at such epochs may lead to widespread obscuration of the AGN emission at UV and optical wavelengths, rendering the detection by ALMA and other long wavelength instruments difficult. Therefore hi-resolution X-ray space observatories, such as ATHENA, will probably be needed to really assess the abundance of such small separation dual AGNs at high- z .

ACKNOWLEDGMENTS

The authors wish to thank Marco Spaans for providing the data tables used for the equilibrium temperature corrections. RR is funded in part by a Marie Curie Career Integration Grant. Part of this research was funded by NASA Award NNX07AH03G. RR also gratefully acknowledges the Aspen Center for Physics, funded by the NSF Grant #1066293, for hospitality during the writing of this manuscript.

REFERENCES

- Agertz O., Teyssier R., Moore B., 2009, *MNRAS*, 397, L64
 Baker J. G., Centrella J., Choi D.-I., Koppitz M., van Meter J., 2006, *Physical Review Letters*, 96, 111102
 Begelman M. C., Blandford R. D., Rees M. J., 1980, *Nature*, 287, 307
 Behroozi P. S., Wechsler R. H., Conroy C., 2013, *ApJ*, 770, 57
 Bournaud F., et al., 2012, *ApJ*, 757, 81
 Bromm V., Ferrara A., Coppi P. S., Larson R. B., 2001, *MNRAS*, 328, 969
 Callegari S., Mayer L., Kazantzidis S., Colpi M., Governato F., Quinn T., Wadsley J., 2009, *ApJL*, 696, L89
 Chapon D., Mayer L., Teyssier R., 2013, *MNRAS*, 429, 3114
 Davies R. I., Tacconi L. J., Genzel R., 2004a, *ApJ*, 602, 148
 Davies R. I., Tacconi L. J., Genzel R., 2004b, *ApJ*, 613, 781
 Elmegreen B. G., Elmegreen D. M., Fernandez M. X., Lomonias J. J., 2009, *ApJ*, 692, 12
 Escala A., Larson R. B., Coppi P. S., Mardones D., 2004, *ApJ*, 607, 765
 Escala A., Larson R. B., Coppi P. S., Mardones D., 2005, *ApJ*, 630, 152
 Fabbiano G., Wang J., Elvis M., Risaliti G., 2011, *Nature*, 477, 431
 Ferrarese L., Merritt D., 2000, *ApJL*, 539, L9
 Fiacconi D., Mayer L., Roškar R., Colpi M., 2013, *ApJL*, 777, L14
 Genzel R., et al., 2006, *Nature*, 442, 786
 Greene J. E., et al., 2010, *ApJ*, 721, 26
 Gültekin K., et al., 2009, *ApJ*, 698, 198
 Häring N., Rix H.-W., 2004, *ApJL*, 604, L89
 Khan F. M., Preto M., Berczik P., Berentzen I., Just A., Spurzem R., 2012, *ApJ*, 749, 147
 Khan F. M., Holley-Bockelmann K., Berczik P., Just A., 2013, *ApJ*, 773, 100
 Klessen R. S., Spaans M., Jappsen A.-K., 2007, *MNRAS*, 374, L29
 Kormendy J., et al., 1997, *ApJL*, 482, L139
 Koss M., et al., 2014, *ArXiv e-prints*,
 Magorrian J., et al., 1998, *AJ*, 115, 2285
 Marconi A., Hunt L. K., 2003, *ApJL*, 589, L21
 Mashchenko S., Wadsley J., Couchman H. M. P., 2008, *Science*, 319, 174
 Mayer L., 2013, *Classical and Quantum Gravity*, 30, 244008
 Mayer L., Kazantzidis S., Madau P., Colpi M., Quinn T., Wadsley J., 2007, *Science*, 316, 1874
 Mayer L., Kazantzidis S., Escala A., 2008, *ArXiv e-prints*, 807
 McConnell N. J., Ma C.-P., 2013, *ApJ*, 764, 184
 Medling A. M., et al., 2014, *ApJ*, 784, 70
 Merloni A., et al., 2010, *ApJ*, 708, 137
 Milosavljević M., Merritt D., 2001, *ApJ*, 563, 34
 Ostriker E. C., 1999, *ApJ*, 513, 252
 Peng C. Y., Impy C. D., Rix H.-W., Kochanek C. S., Keeton C. R., Falco E. E., Lehár J., McLeod B. A., 2006, *ApJ*, 649, 616
 Pérez F., Granger B. E., 2007, *Computing in Science and Engineering*, 9, 21
 Pontzen A., Roskar R., Stinson G., Woods R., 2013, *pynbody: N-Body/SPH analysis for python*, ascl:1305.002
 Reines A. E., Sivakoff G. R., Johnson K. E., Brogan C. L., 2011, *Nature*, 470, 66
 Reines A. E., Greene J. E., Geha M., 2013, *ApJ*, 775, 116
 Sanders D. B., Mirabel I. F., 1996, *ARA&A*, 34, 749
 Sani E., Marconi A., Hunt L. K., Risaliti G., 2011, *MNRAS*, 413, 1479
 Schawinski K., Simmons B. D., Urry C. M., Treister E., Glikman E., 2012, *MNRAS*, 425, L61
 Spaans M., Silk J., 2000, *ApJ*, 538, 115
 Springel V., Di Matteo T., Hernquist L., 2005, *MNRAS*, 361, 776
 Stadel J. G., 2001, PhD thesis, AA(UNIVERSITY OF WASHINGTON)
 Stinson G., Seth A., Katz N., Wadsley J., Governato F., Quinn T., 2006, *MNRAS*, 373, 1074
 Tremaine S., et al., 2002, *ApJ*, 574, 740

- Van Wassenhove S., Volonteri M., Mayer L., Dotti M., Bellovary J., Callegari S., 2012, *ApJL*, 748, L7
- Van Wassenhove S., Capelo P. R., Volonteri M., Dotti M., Bellovary J. M., Mayer L., Governato F., 2014, *MNRAS*, 439, 474
- Wada K., 2001, *ApJL*, 559, L41
- Wada K., Norman C. A., 2001, *ApJ*, 547, 172
- Wadsley J. W., Stadel J., Quinn T., 2004, *New Astronomy*, 9, 137